Many-Body Effects in the Formation of Multiply Charged Ions in a Strong Laser Field

B. A. Zon[a,b,*], A. S. Kornev[a,], and E. B. Tulenko[a,***]**

[a] *Voronezh State University, Voronezh, 394006 Russia*

[b] *Belgorod State University, Belgorod, 308015 Russia*

Abstract—Some of the many-body effects in the formation of multiply charged ions in a laser field have been taken into account: inelastic tunneling, collective tunneling, and magnetic moment projection relaxation of the atomic core. Strong fields with an intensity exceeding 10^{17} W cm^{-2} are considered when the magnetic component of the laser field acts on the free motion of a photoelectron; therefore, the formation of multiply charged ions through rescattering becomes unlikely. Numerical calculations have been performed for Ar^{9+}... Ar^{13+}, Kr^{19+}... Kr^{23+}, Rb^{10+}, and Rb^{11+} ions. A significant contribution of collective tunneling, which was not observed in weaker fields investigated previously, has been revealed. Allowance for collective tunneling is shown to reduce the intensity leading to saturation by more than 10%. In this case, the yield of multiply charged Rb ions changes by an order of magnitude, while the yield of multiply charged Ar and Kr ions changes by more than a factor of 2. Comparison with experimental data on the formation of argon ions under the action of a linearly polarized laser pulse is made.

1. INTRODUCTION

In recent years, the formation of multiply charged atomic ions (MCIs) in a superstrong laser field with an intensity as high as 10^{19} W cm^{-2} has been actively studied experimentally [1–8]. Relativistic effects begin to manifest themselves in such intense fields. The first effect of this kind is related to the action of the magnetic component of the laser light field on the motion of a free electron. This effect should be considered as relativistic, because the Lorentz force is known to be inversely proportional to the speed of light. As a result of the action of the Lorentz force, the motion of an electron in the field of a light wave ceases to be rectilinear; its trajectory takes a figure-of-eight shape [9]. As a consequence, the rescattering processes, which played a major role in the formation of multiply charged ions in less intense fields [10, 11] when impact ionization took place as a result of photoelectron acceleration in a laser field with the formation of higher-charge ions, now become less significant. An experimental confirmation of the suppression of rescattering by relativistic effects was pointed out in [1, 2, 4] and was studied most extensively in [7].

Since the rescattering process ceases to be dominant, multiply charged ions are formed through the direct action of a laser field on an atom or ion. The existing tunneling theory [12–15], known as the ADK theory, along with its relativistic generalization [16, 17], is a single-body one. Therefore, the formation of multiply charged ions in this theory is possible only through the sequential detachment of each electron from a neutral atom or ion with the formation of a higher-charge ion in the ground state. Obviously, in this respect, it is desirable to improve the ADK theory by including many-body effects.

Previously, we performed the works [18, 19] in this direction. We considered lower laser intensities, when no relativistic effects manifested themselves as yet. To eliminate the rescattering effects, the laser field as assumed to be circularly polarized. We took into account the following many-body effects: (1) the inelastic tunneling effect (ITE) accompanied by ionic core excitation [20]; and (2) the collective tunneling of several electrons in one optical half-cycle [21] (see also [22]). The results of our calculations for Ne^{2+} [19] agree well with the experimental results from [23]. The results of our theoretical calculations of the formation probability of Ar^{+}... Ar^{6+} ions [18] were subsequently verified experimentally in [24]. Circularly polarized radiation with an intensity of 10^{14}–10^{16} W cm^{-2} was used in this paper. The experimental data obtained were presented for a spatially homogeneous laser beam, which allowed a decrease in the formation probability of ions of charge n due to the formation of higher-charge ions from them to be observed. Recall that such a decrease cannot be observed for a Gaussian

intensity distribution in the laser beam. All of the experimental data from [24] agree excellently with the results of our calculations [18].

From the viewpoint of the role of many-body effects in the formation of multiply charged ions, the results of [18, 24] confirm the importance of the inelastic tunneling effect. As regards the collective tunneling effect, it did not manifest itself at the above intensities of 10^{14}–10^{16} W cm^{-2}. As was shown recently [25] with the formation of Rb^{10+} and Rb^{11+} ions in a linearly polarized field, the role of collective tunneling in the formation of MCIs becomes important if the intensity required for their production exceeds 10^{17} W cm^{-2}.

Yet another many-body effect was investigated in [25], electron magnetic quantum number m relaxation of the atomic core, which was studied theoretically [26] and experimentally [27]. The relaxation time was shown to be much shorter than the laser pulse duration, in agreement with the experimental data [27].

The goal of this paper is to further study the formation of multiply charged ions in terms of the many-body tunneling theory in fields with an intensity as high as 10^{19} W cm^{-2}. The laser radiation is assumed to be linearly polarized, because, as was said above, the processes of ionization through rescattering are suppressed as a result of the action of the Lorentz force on a free electron.

In the next section, we provide general formulas that describe the probability of the collective inelastic tunneling effect. In accordance with the results of [16, 17], the tunneling process for ion charges $\lesssim 20$ may be considered in the nonrelativistic approximation. The kinetic equations that describe the MCI formation with allowance made for the many-body effects are given in Section 3. The results of our calculations of the formation probabilities of Ar^{9+}...Ar^{13+}, Kr^{19+}...Kr^{23+}, Rb^{10+}, and Rb^{11+} ions both for a spatially homogeneous laser beam and for a beam with a Gaussian intensity distribution are presented in Section 4. The theoretical results are compared with the available experimental data in Section 5. We show that the single-body model occasionally leads to qualitative differences between theory and experiment.

Unless stated otherwise, the atomic system of units ($\hbar = m_e = e = 1$) is used everywhere.

2. THEORETICAL DESCRIPTION OF MANY-BODY EFFECTS

The quantum defect approximation well known in atomic and molecular physics [28] underlies the single-body ADK tunneling theory. The applicability of the quantum defect theory to the ground and low-lying atomic states is justified in [29]. The rate of the collective tunneling of several equivalent electrons used here was obtained in [21]. Another many-body effect, core excitation as a result of single-electron tunneling, was taken into account in [20]. A similar inelastic tunneling effect was obtained in [20] in Carlson's approximation [30], who considered single-photon two-electron helium ionization. Since the change of the self-consistent field in the outer shell is disregarded, the excited states of the residual ion are different components of the fine structure of the same multiplet to which the ground state of the residual ion also belongs. Agreement between theory and experiment [18, 24] shows that this approximation is quite satisfactory for the problem under consideration.

Both many-body effects (collective and inelastic tunneling) can be described by one formula given in [18] for circularly polarized radiation. For linearly polarized radiation, the rate of inelastic collective tunneling of N equivalent electrons from the shell of a neutral atom or a positive ion is given by the expression[1]

$$W^{(N,\mathrm{lin})}_{\kappa l\{m\}} = \sqrt{\frac{6}{\pi}}\frac{M!\left(l+\frac{1}{2}\right)^N}{2^M N^{M+7/2}} C^{2N}_{\kappa l} Q^2 \kappa^{3N-1} \times \left(\frac{2F_a}{F}\right)^{2(Z/\kappa-1)N-M+1/2} \exp\left(-\frac{2NF_a}{3F}\right) \times \prod_{j=1}^{N}\frac{(l+m_j)!}{m_j!^2(l-m_j)}. \quad (1)$$

Here, the index $\{m\}$ denotes the set of orbital angular momentum projections of the emitted electrons (m_1, m_2, ..., m_N), so that

$$M = \sum_{j=1}^{N}|m_j|,$$

l is the orbital quantum number of the electron,

$$\kappa = \sqrt{\frac{2E^{(N)}}{N}}, \quad E^{(N)} = \sum_{j=1}^{N} E_j,$$

$$E_j = E_j^{(0)} - \Delta_j,$$

$E_j^{(0)}$ is the jth ionization potential of the initial atom (or ion), Δ_j is the core excitation energy, $F_a = \kappa^3$ is the characteristic intraatomic field strength, F is the amplitude of the laser wave electric field strength, Z is the charge of the residual ion, and Q is the overlap integral. The overlap integrals in the LS-coupling scheme are calculated in Appendices A and B.

The constant $C_{\kappa l}$ in Eq. (1) is defined by the asymptotic behavior of the single-electron wave function for a free atom (or ion) at $r \gg 1$:

$$\psi(\mathbf{r}) \approx C_{\kappa l}\kappa^{3/2}(\kappa r)^{N\left(\frac{Z}{\kappa}-1\right)} e^{-\kappa r} Y_{lm}(\hat{\mathbf{r}}).$$

[1] The erratum made in [18] in the exponent N in the pre-exponential factor was removed in Eq. (1).

The most accurate method for calculating $C_{\kappa l}$ is direct numerical integration of the Hartree–Fock equations for a free atom. Knowledge of the Rydberg atomic or ionic spectrum for the entire series under consideration [31] is required to calculate $C_{\kappa l}$ in the quantum defect approximation. No such information is available for the multiply charged ions we investigated [32]. Therefore, in this paper, we used a semiclassical formula from [21] whose accuracy can be judged from the results presented in [31]:

$$C_{\kappa l} = \frac{(2/\nu)^{\nu}}{\sqrt{2\pi\nu}}\left(\frac{1-\varepsilon}{1+\varepsilon}\right)^{(l+1/2)/2}(1-\varepsilon^2)^{-\nu/2}. \quad (2)$$

Here, $\nu = Z/\kappa$, $\varepsilon = (l+1/2)/\nu$ is the eccentricity of the classical electron orbit. Equation (2) was derived for $\varepsilon < 1$. At $\varepsilon > 1$, the semiclassical approximation is inapplicable and numerical methods are required to obtain $C_{\kappa l}$.

The applicability conditions for Eq. (1) are the smallness of the square of the N-body Keldysh parameter:

$$\gamma^2 = \frac{\omega^2}{F^2}\frac{2E^{(N)}}{N} \ll 1, \quad (3)$$

where ω is the radiation frequency, and the smallness of the external field strength compared to the intraatomic one:

$$F \ll F_a. \quad (4)$$

The satisfaction of condition (3) provides tunneling ionization under which the ionization rate does not depend on the radiation frequency. Condition (4) allows the influence of the light field on the bound electron to be disregarded, which is used in deriving Eq. (1). Note that for highly excited (Rydberg) states with high ν, condition (4) can be replaced by a more rigorous one due to the switch-on of above-barrier ionization (for a more detailed discussion, see [21]). The states of the parent and residual ions are taken into account in Eq. (1) via the parameters κ and Q.

The role of the magnetic quantum number m in the formation of multiply charged ions was discussed in [26]. According to the data from this paper, electrons with a zero total angular momentum projection onto the direction of the electric field of linearly polarized laser radiation are emitted at the leading edge of the laser pulse. Electrons with $|m| > 0$ are emitted at a higher radiation intensity. As a result, a peculiar angular distribution of photoelectrons emerges. However, the experimental data from [27] indicate that fast m relaxation of the remaining electrons in the ionic core takes place as a result sequential ionization.

The fast relaxation observed in [27] may be attributable to the electrostatic interaction of electrons from the shell under consideration, which gives rise to a general orbital angular momentum of the shell L (in the LS-coupling scheme). To estimate its rate, we will use the quantum energy–time uncertainty relation. Assuming the ionic level spacing to be ~1 eV (see Table 1), we will obtain the following estimate for the m-relaxation time: $\tau_{relax} \approx 6 \times 10^{-16}$ s. This is much shorter than both the laser pulses experimentally used in [27], about 40 fs, and the pulses considered here.

The assumption about fast m relaxation is actually contained in Eq. (1), because the presence of overlap integrals in (1) suggests the formation of LS states in times much smaller than the inverse probability of the tunneling effect.

3. KINETIC EQUATIONS

In this paper, the tunneling formation of MCIs is considered as a multichannel cascade process. It includes both single-electron and collective tunneling cascade transitions that can be accompanied by ionic core excitation. Significantly, the number of cascade channels increases rapidly with ion charge. In addition, the emitted electrons can have different orbital angular momentum projections m, which, in turn, leads to a further branching of the cascade process.

The multiple tunneling ionization of neutral atoms under the action of a laser pulse is described by a system of kinetic equations for the populations of various ionic states C_f [18]:

$$\frac{dC_f}{dt} = \sum_{f'=0}^{f-1} W_{f'\to f}C_{f'} - \sum_{f'=f+1}^{f_{tot}} W_{f\to f'}C_f, \quad (5)$$

$$f = 0, 1, \ldots, f_{tot},$$

$$C_0(-\infty) = 1, \quad C_1(-\infty) = \ldots = C_{f_{tot}}(-\infty) = 0. \quad (6)$$

The indices f and f' in Eqs. (5) number the ionic states with charges Z and Z', respectively, including the excited ionic states that correspond to the inelastic tunneling effect; f_{tot} is the number of involved ionic states. $W_{f'\to f}$ is the tunneling transition rate from state $|f'\rangle$ to state $|f\rangle$ obtained from Eq. (1) by replacing the monochromatic field strength F with the pulse envelope $F(t)$. The first term in Eqs. (5) correspond to an increase in the population of state $|f\rangle$ with charge Z through the ionization of lower-Z' ions and, hence, the first sum over f' extends only to the states with $Z' < Z$. The second term in (5) corresponds to a decrease in the population of state $|f\rangle$ through its further ionization and, hence, the second sum over f' contains only the states with $Z' > Z$. Equations (5) disregard the recombination through the broadening of the wave packet of photoelectrons as it moves in the laser field.

Below, we will be interested in the ionization of electrons with an orbital quantum number l at a laser intensity higher than 10^{17} W cm^{-2}. The outer shells of neutral atoms are completely ionized in the range 10^{14}–10^{16} W cm^{-2} [18, 19]. Therefore, all atoms ahead of the leading edge of the pulse may be considered ionized up to the term $l^{2(2l+1)}(^1S_0)$. Thus, the states

Table 1. Parameters of the outer shells of Ar^{8+} ... Ar^{14+} and Kr^{18+} ... Kr^{24+} ions

X	Outer shell		Ionization (italics) and excitation energies [32]	
			$Ar^{(8+X)+}$	$Kr^{(18+X)+}$
0	p^6	$^1S_0$	0	0
1	p^5	$^2P_{3/2}$	*31.056*	*63.00500*
		$^2P_{1/2}$	0.16462	0.912269
2	p^4	$^3P_2$	*35.256*	*66.54072*
		$^3P_1$	0.13171	0.82898
		$^3P_0$	0.16683	0.45727
		$^1D_2$	0.65459	1.16806
		$^1S_0$	1.3533	2.28655
3	p^3	$^4S_{3/2}$	*39.691*	*70.47648*
		$^2D_{3/2}$	0.86407	0.78805
		$^2D_{5/2}$	0.89439	1.07910
		$^2P_{1/2}$	1.35941	1.51581
		$^2P_{3/2}$	1.4038	2.19851
4	p^2	$^3P_0$	*45.476*	*75.24332*
		$^3P_1$	0.08984	0.72910
		$^3P_2$	0.19911	0.980797
		$^1D_2$	0.77487	1.92168
		$^1S_0$	1.47751	2.57242
5	p^1	$^2P_{1/2}$	*50.41*	*79.41054*
		$^2P_{3/2}$	0.20647	1.01278
6	p^0	$^1S_0$	*55.506*	*82.67926*

$|l^k(aSL)JM_J\rangle$ correspond to the indices f and f' (see Appendix A). In particular, the state $|l^{2(2l+1)}(^1S_0)00\rangle$ should be understood by $f = 0$ here. The quantity C_f should be considered as the ratio of the number density of ions n_f in state $|f\rangle$ to the number density of neutral atoms n_{tot} in the gaseous target or $n_0 = n_{\text{tot}}$ ahead of the leading edge of the pulse:

$$C_f(t) = \frac{n_f(t)}{n_0(-\infty)}, \quad \sum_{f=0}^{f_{\text{tot}}} n_f(t) = n_0(-\infty).$$

Since the initial conditions (6) are formulated for an instant of time preceding the laser pulse arrival, $-\infty$ is formally present in the arguments of C_f. The result of integrating Eqs. (5) is the set of $C_f(\infty)$ values that define the number density of ions in each state after laser pulse termination.

4. RESULTS OF OUR CALCULATIONS AND THEIR DISCUSSION

In this section, we present the results of integrating the kinetic equations (5) that describe the formation of multiply charged ions under the action of a laser pulse with a Gaussian envelope,

$$F(t) = F_0 \exp\left(-\frac{t^2 \ln 2}{T^2}\right),$$

where F_0 is the maximum electric field strength and T is the duration or the time in which the pulse envelope is reduced by half. In this case, it will suffice to replace the argument $-\infty$ by $-2T$ in the initial conditions (6) and to take $2T$ as the upper limit of integration. The output parameters $C_f(2T)$ are functions of the peak intensity I_0 in the pulse.

The calculations were performed for Ar^{9+}...Ar^{13+}, Kr^{19+}...Kr^{23+}, and Rb^{10+}... Rb^{12+} ions in a gaseous target as a function of the peak intensity in a linearly polarized laser pulse with durations of 2 (for argon and krypton) and 5 (for rubidium) fs. For krypton ions, the $3d$ shell is assumed to be completely ionized: as can be seen from the experimental data for xenon ions [4], the formation of Xe^{19+} with the outer p shell begins virtually in the saturation regime of Xe^{18+} with the outer d shell, because the ionization potentials of the p shell are more than twice those of the d one. We took into account the single-, two-, and three-electron collec-

tive transitions between all of the states listed in Tables 1 and 2. Only the excited states in which the principal quantum numbers do not change are taken into account. Otherwise, the excitation energies increase by one or two orders of magnitude, becoming comparable to the ionization potentials and leading to an exponential decrease in the corresponding probabilities. A similar situation also takes place for Ar^{9+}...Ar^{13+} and Kr^{19+}...Kr^{23+} ions with the outer p shell.

4.1. The Populations of Charge States

Let us introduce the number density of ions with a given charge X in all states of the l shell $|f_1(X)\rangle$, $|f_2(X)\rangle$, ..., $|f_{\max}(X)\rangle$:

$$n(A^{X+}) = \sum_{f=f_1(X)}^{f_{\max}(X)} n_f. \qquad (7)$$

By analogy with (7), we can introduce the number density of ions with a given electronic term $n[A^{X+}(aSLJ)]$. In all cases, the summation over all angular momentum projections is implied in Eq. (7). In this paper, $n(A^{X+})$ are calculated as functions of the peak intensity I_0 in the pulse after its termination. The results obtained in this way are valid for a spatially homogeneous laser beam with an infinitely large focal diameter.

Figures 1 and 2 present the results of our calculations of $n(Ar^{9+})$...$n(Ar^{13+})$ and $n(Kr^{19+})$...$n(Kr^{23+})$. The results were divided into two groups. The first group includes only the sequential single-electron transitions between the ground ionic states (the ADK model). In this case, 15 charged states are involved in the kinetic equations (5) and the number of possible ionization channels reaches 80. The second group corresponds to all of the possible single-electron transitions, including the ITE. The third group additionally includes the collective two-electron tunneling transitions. In these cases, 61 charge states are involved in kinetic equations (5) and the number of possible ionization channels exceeds 10^5. The three-electron collective tunneling effect in the investigated channels does not affect significantly the result and, therefore, is not presented in the figures.

As with the lower-charge ions of the same atoms [18, 19], allowance for the core excitation has virtually no effect on the ionization of the first shell electron in the region of increase in the population of Ar^{9+} and Kr^{19+} ions. Similar to the results of [18, 19], the difference from the ADK model by one or two orders of magnitude manifests itself only when the second electron in the shell is ionized (Ar^{10+} or Kr^{21+}), which is the result of a rapid increase in the number of ionization channels. In contrast to the results of [18, 19], the two-electron collective ITE becomes noticeable for higher-charge ions. It manifests itself in the formation of Ar^{10+} and Kr^{21+} ions and for higher-charge ions.

Table 2. Parameters of the outer shells of Rb^{9+} ... Rb^{12+} ions: ionization (italics) and excitation energies [32]

Ion	Outer shell		Energy, Ry
Rb^{9+}	$3d^{10}$	$^1S_0$	*20.32126*
Rb^{10+}	$3d^9$	$^2D_{5/2}$	*23.14618*
		$^2D_{3/2}$	0.11263
Rb^{11+}	$3d^8$	$^3F_4$	*26.88238*
		$^3F_3$	0.10006
		$^3F_2$	0.14225
		$^1D_2$	0.31001
		$^3P_1$	0.42447
		$^3P_0$	0.43030
		$^3P_2$	0.43805
		$^1G_4$	0.52562
		$^1_0S_0$	1.15977
Rb^{12+}	d^7	$^4F_{9/2}$	*30.70970*
		$^4F_{7/2}$	0.08779
		$^4F_{5/2}$	0.13906
		$^4F_{3/2}$	0.17050
		$^4P_{3/2}$	0.36396
		$^4P_{5/2}$	0.39124
		$^2G_{9/2}$	0.40867
		$^2G_{7/2}$	0.49097
		$^2H_{11/2}$	0.55505
		$^2H_{9/2}$	0.64263
		$^2D_{5/2}$	0.58273
		$^2D_{3/2}$	0.72273
		$^2F_{5/2}$	0.87492
		$^2F_{7/2}$	0.919933
		$^2_1D_{3/2}$	1.35396
		$^2_1D_{5/2}$	1.39998

Whereas for argon the contribution from the two-electron process exceeds that from the single-electron one by a factor of 2–2.5, for krypton and, accordingly, a higher radiation intensity this difference can reach one order of magnitude. The difference between the single and two-electron ITEs for Ar^{10+} and Kr^{20+} ions manifests itself only in the region of decrease in the population. Note that the two-electron ITE manifested itself very insignificantly in the populations of the charge states of Ar^{1+}...Ar^{5+} and Kr^{1+}...Kr^{5+} far from the saturation points.

No further ionization of Ar^{14+} and Kr^{24+} is considered in the approximation we used, because no spectroscopic information about the excited states of these ions is available. Nevertheless, their further ionization

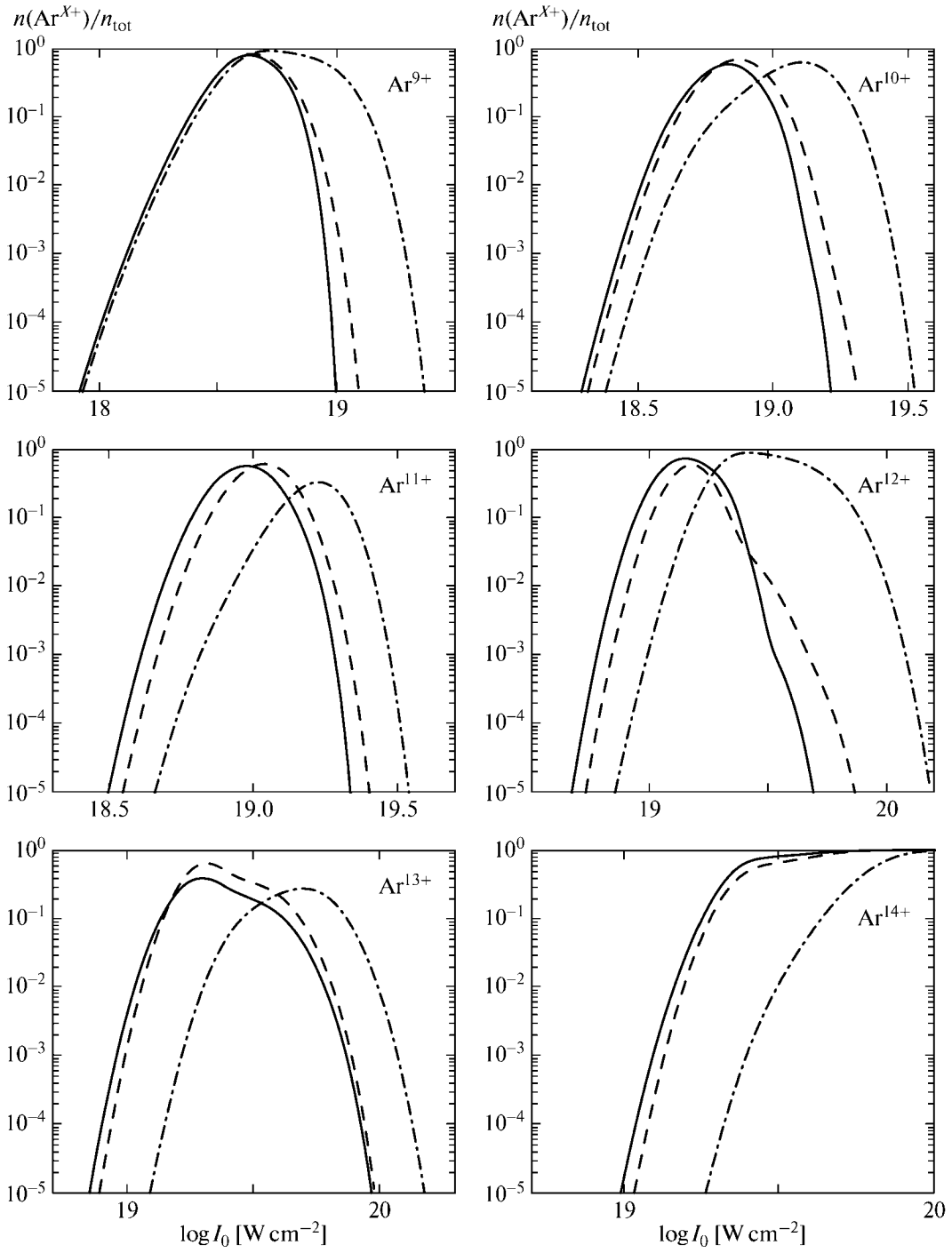

Fig. 1. Ratio of the number density of Ar^{X+} MCIs with the $[He]2s^2 2p^{6-X}$ configuration to the number density of neutral atoms before the action of a laser pulse with duration $T = 2$ fs versus peak intensity of the pulse. The solid, dashed, and dash–dotted curves correspond to allowance for the single- and two-electron transitions with core excitation, only the sequential single-electron transitions with core excitation, and the sequential single-electron transitions between the ground MCI states (the ADK model), respectively.

is also possible, as was shown in an argon ionization experiment [3]. The results on the yield of Ar^{14+} and Kr^{24+} MCIs are presented here only for illustration and cannot be used for comparison with the experiment.

Note that the Ar^{13+} and Kr^{23+} populations (Figs. 1 and 2, respectively) calculated by taking into account only the single-electron sequential inelastic tunneling transitions exceed considerably those obtained by taking into account the two-electron collective tunneling

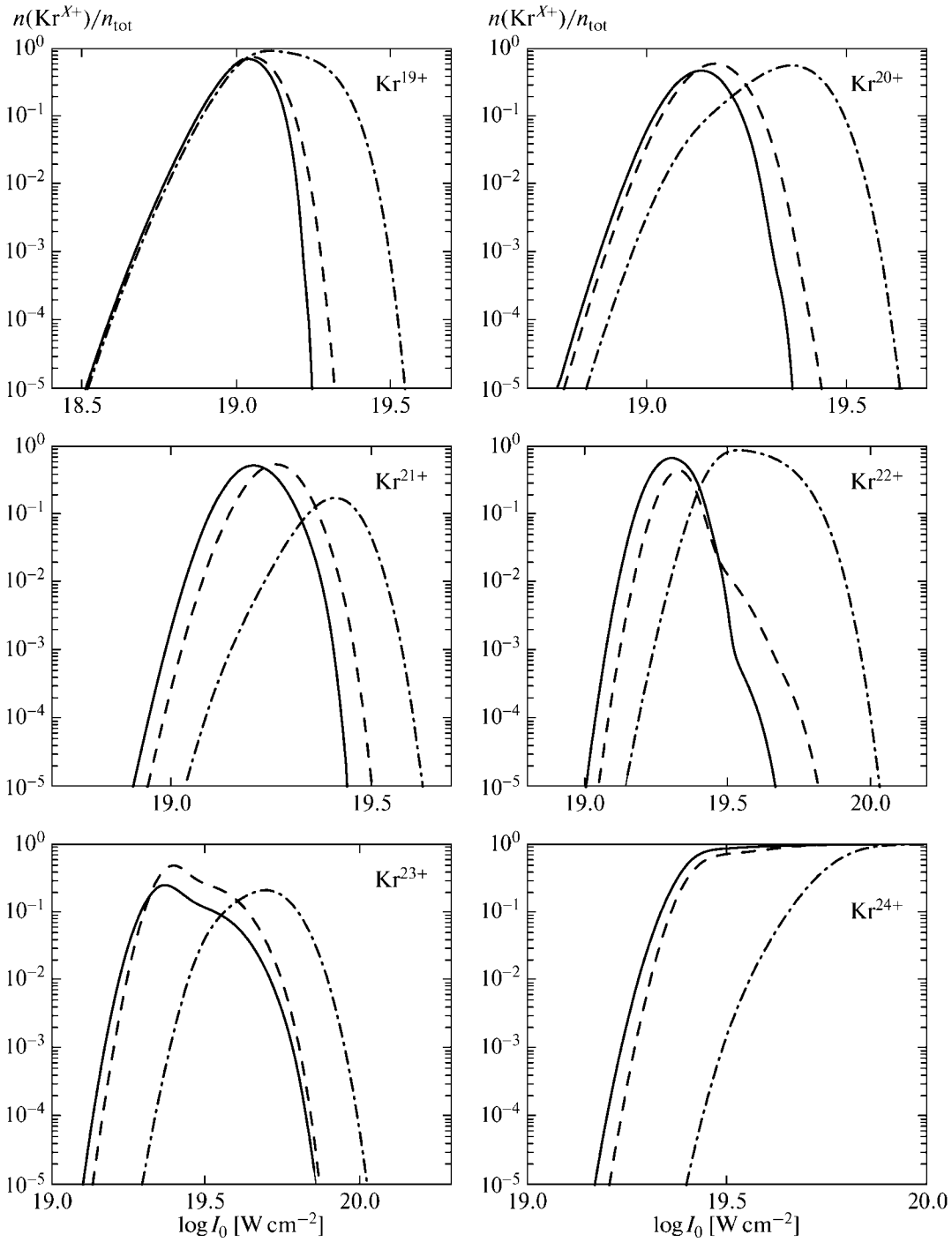

Fig. 2. Same as Fig. 1 for Kr^{X+} ions with the $[Ne]3s^23p^{6-X}$ configuration.

effect. This fact can be explained by a growing probability of the two-electron $Ar^{12+} \longrightarrow Ar^{14+}$ and $Kr^{22+} \longrightarrow Kr^{24+}$ transitions with increasing laser intensity. A similar situation also takes place for Ar^{10+} and Kr^{20+} ions, but the effect is less pronounced in this case.

For completeness, we will present the populations of the Rb^{10+} and Rb^{11+} states in a gaseous target at $T =$ 5 fs calculated in our recent paper [25] (see Fig. 3). In these states, one and two electrons, respectively, were removed from the closed d shell. These MCIs are formed at a lower intensity than that for argon due to the lower ionization potentials. Therefore, the difference between the single-electron and two-electron collective tunneling effects is less pronounced here

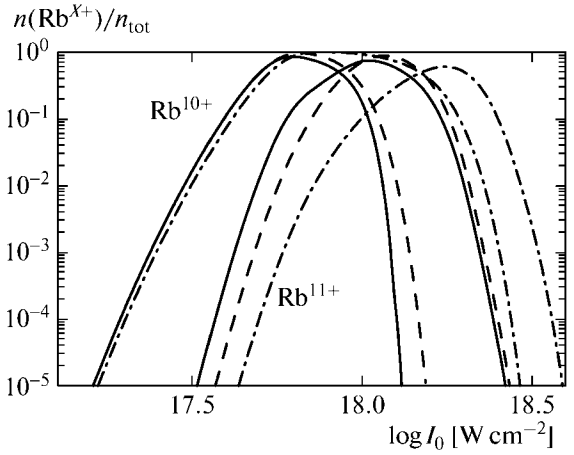

Fig. 3. Same as Fig. 1 for Rb^{X+} ions with the $[Ar]3d^{19-X}$ configuration.

than that for argon. At $T = 40$ fs, the collective tunneling effect is barely noticeable [25] and the results are not presented here.

In the case of rubidium for the ADK model, 20 charge states are involved in the kinetic equations (5) and the number of possible ionization channels reaches 210. In the many-body model, 173 charge states are involved in the kinetic equations (5) and the number of possible ionization channels exceeds 50000.

In [25], we also calculated the contribution from individual multiplets to the formation of Rb^{10+} and Rb^{11+} MCIs at $T = 5$ fs. Similar results can also be obtained for the investigated argon and krypton ions.

In [21], it was pointed out that two-electron collective tunneling could be more probable than sequential single-electron tunneling. This is attributable to the structure of the exponential factors in Eq. (1). However, given the saturation of the number density of lower-charge ions and the pre-exponential factors in (1), no unambiguous conclusion regarding the appearance of collective tunneling can be reached without detailed calculations.

In real situations, the radiation intensity in the laser beam is not spatially homogeneous. A procedure for reducing the experimental results to a spatially homogeneous intensity distribution was proposed in [33]. It is based on intensity selective scanning in the laser beam [34]. This procedure was used in [24] to measure the populations of Ar^{1+}...Ar^{5+} ions after the action of a pulse of circularly polarized radiation with $T = 50$ fs and a central wavelength of 790 nm on the gas. This experiment completely confirmed the many-body tunneling theory [18] used here.

4.2. Ion Yields in a Gaussian Beam

Let us now calculate the yield of multiply charged ions in the case of a realistic laser intensity distribution corresponding to a focused beam with diffraction. In most experiments (see, e.g., [27]), the ions are extracted from the entire focal volume and not from its individual elements [34]. Therefore, apart from the population, it is necessary to obtain the absolute number of ions in given states in the focal volume.

Consider a focused laser beam with a Gaussian distribution of the peak intensity over the diameter:

$$I(\mathbf{r}) = I_b(z)\exp\left[-\frac{2r^2}{r_b^2(b)}\right], \tag{8}$$

where

$$r_b(z) = r_0[1 + (z/z_0)^2]^{1/2},$$

$$I_b(z) = I_a[1 + (z/z_0)^2]^{-1},$$

r_0 is the beam waist radius, I_a is the peak intensity on the beam axis at the waist point (absolute intensity), z_0 is the Rayleigh parameter given by the relation $z_0 = \pi r_0^2/\lambda$, λ is the laser wavelength. If we integrate the population $C_f(I(\mathbf{r}))$ over the beam volume, then we will obtain the integrated ion yield:

$$P_f(I_a) = n_{tot}\int C_f(I(\mathbf{r}))d^3r = \frac{n_{tot}}{\lambda}(\pi r_0^2)^2 \times \int_0^\infty d\zeta(1+\zeta^2)\int_0^{I_a/(1+\zeta^2)} C_f(I')\frac{dI'}{I'}, \tag{9}$$

where $\zeta = z/z_0$. Quantity (9) has the meaning of the absolute number of ions in state $|f\rangle$ inside the focal volume. By analogy with (7), we will introduce the yield of ions $P(A^{X+})$ with charge X in all of the possible states of the electronic shells. In accordance with [35], $P(I_a) \sim I_a^{3/2}$ in the saturation region due to the combined influence of the decrease in the number of MCIs in a given state and the increase in the focal volume.

$P(Ar^{9+})$...$P(Ar^{13+})$ and $P(Kr^{19+})$...$P(Kr^{23+})$ are plotted against the absolute intensity I_a at $T = 2$ fs in Figs. 4 and 5, respectively. The spatial averaging here still retains a noticeable difference between the one and two-electron ITEs in several cases. In contrast to the formation of lower-charge MCIs with lower ionization potentials [18, 19, 25], it is convenient to compare the groups of results in this case by the location of the saturation boundary. For example, for argon, allowance for the two-electron ITE causes the saturation boundary in Ar^{11+}, Ar^{12+}, Kr^{21+}, and Kr^{22+} to be lowered by more than 10%. In this case, the yield of Ar^{12+} and Kr^{22+} MCIs increases by more than a factor of 2.

In the literature, there are experimental data on the yield of argon MCIs as a function of the absolute intensity only up to a charge of 9+ at $T = 25$ fs [6]. However, only the first shell electron is ionized in such MCIs. As we showed in [19], in this case, good agree-

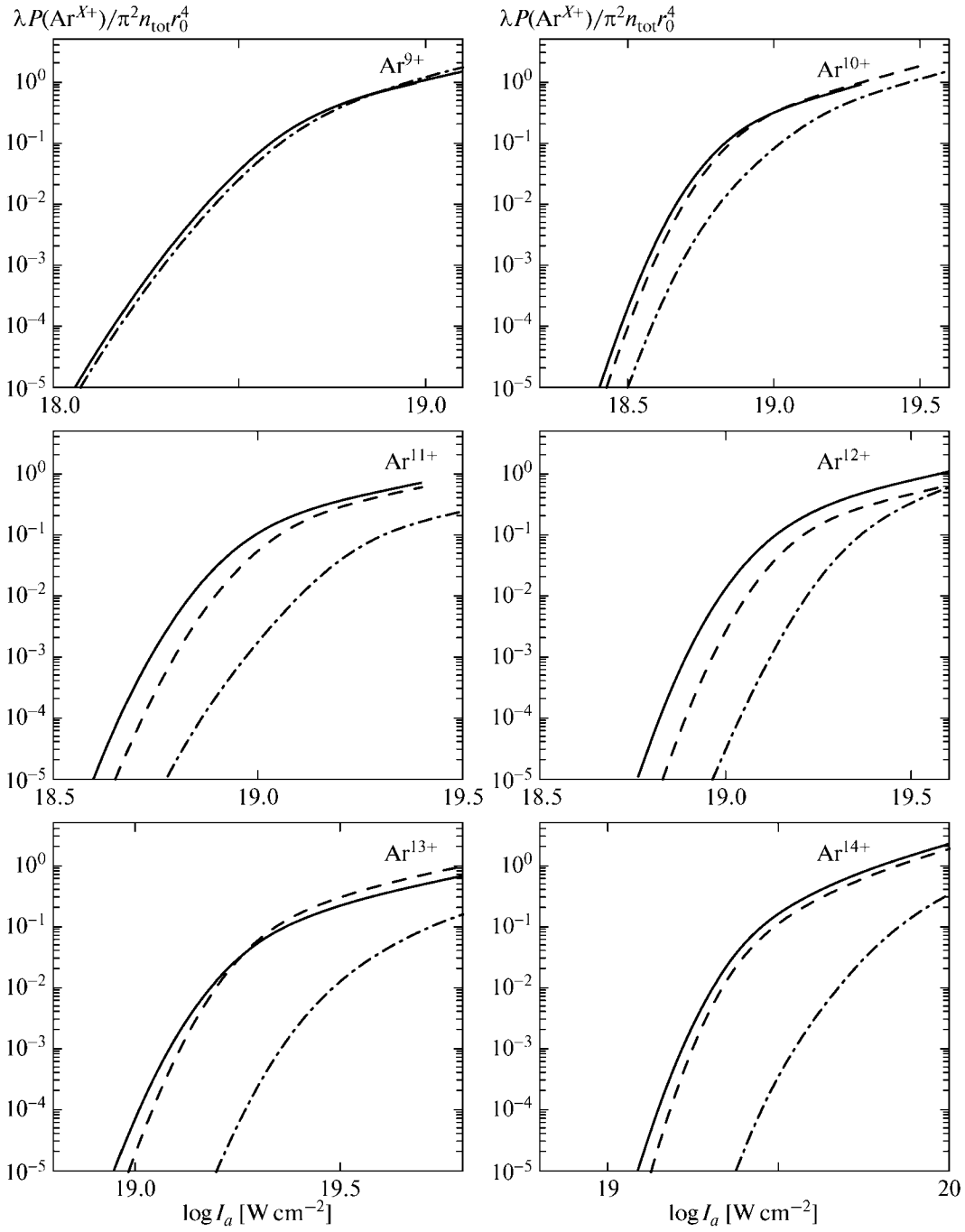

Fig. 4. Yield of Ar^{9+}... Ar^{14+} ions integrated over the focal volume. The notation is the same as that in Fig. 1.

ment with the experiment can be achieved in this case by slightly shifting the plot along the intensity axis (~5%). Only after such "calibration" can a comparison be made with the experiment for ions with shells without two, three, or more electrons (in our case, for Ar^{10+}, Ar^{11+}, etc.).

The available experimental data for krypton were obtained only for MCIs with the outer *d* shell [3, 7, 27]. There is no spectroscopic information for them [32] and their yields cannot be calculated in terms of the model under consideration. Note, however, that the authors of [7, 27] have already pointed out the difference between their experimental data and the ADK model results. The absence of spectroscopic data for highly charged MCIs does not allow the corresponding calculations to be performed either despite the performed experiments [3, 6, 36].

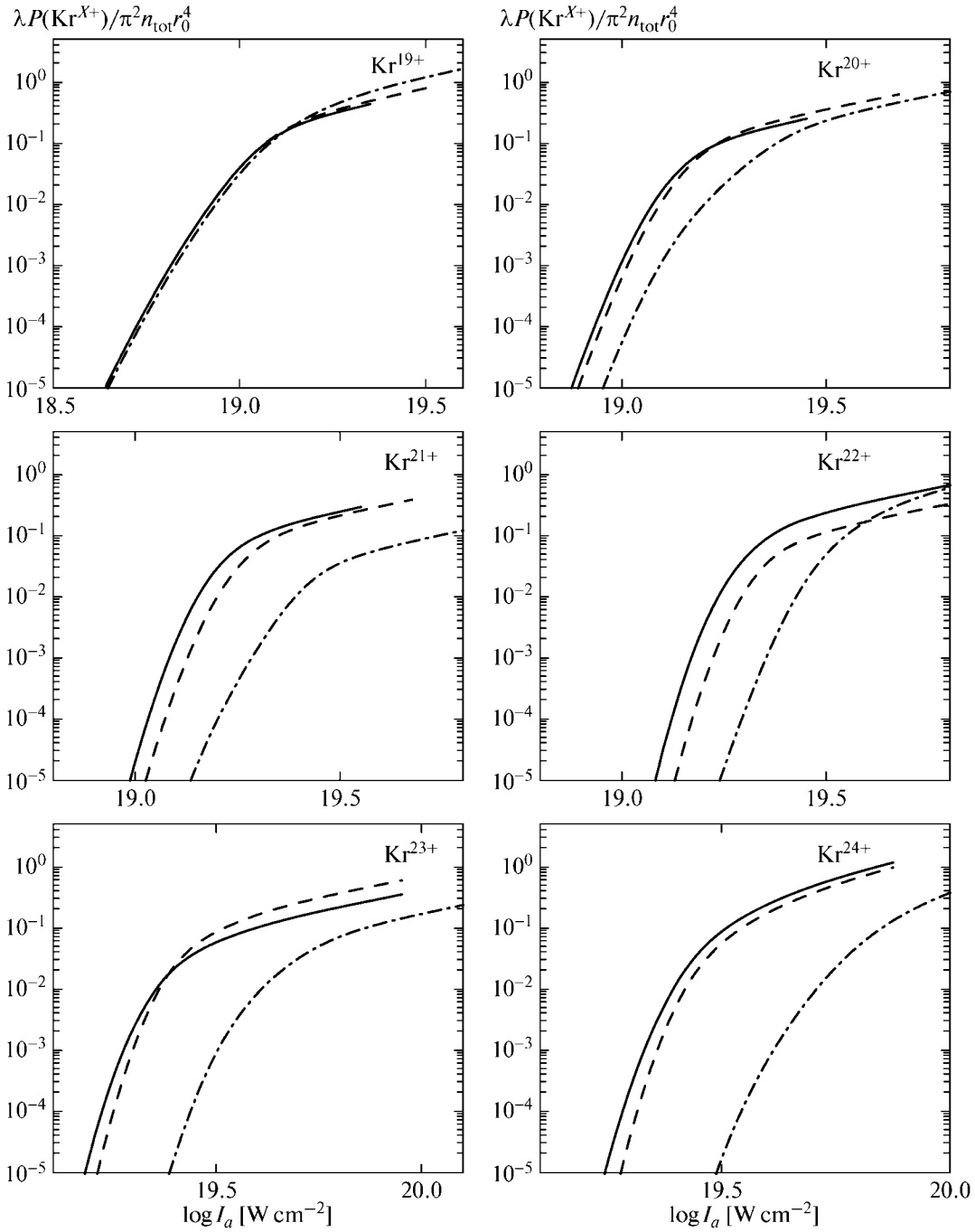

Fig. 5. Yield of Kr^{19+}...Kr^{24+} ions integrated over the focal volume. The notation is the same as that in Fig. 1.

$P(Rb^{10+})$ and $P(Rb^{11+})$ are plotted against the absolute intensity I_a at $T = 5$ fs in Fig. 6 (taken from [25]). The spatial integration here still retains a noticeable difference between the one- and two-electron ITEs. This difference decreases with decreasing radiation intensity. Unfortunately, rubidium is currently the only element with the outer d shell with spectroscopic data (the configuration of terms and the ionization energies) available for its ions [32].

5. COMPARISON WITH THE EXPERIMENT

Among the multiply charged ions investigated here, Ar^{9+}, Ar^{11+}, Ar^{12+}, and Ar^{13+} were produced in the experiment [3]. The authors of [3] used a titan–sapphire laser with a central wavelength of 800 nm and pulse duration $T = 25$ fs. As we showed in [25] for Rb^{9+}...Rb^{11+}, no collective tunneling manifests itself at such radiation parameters. Therefore, to compare the theory with the experiment, we restricted ourselves to

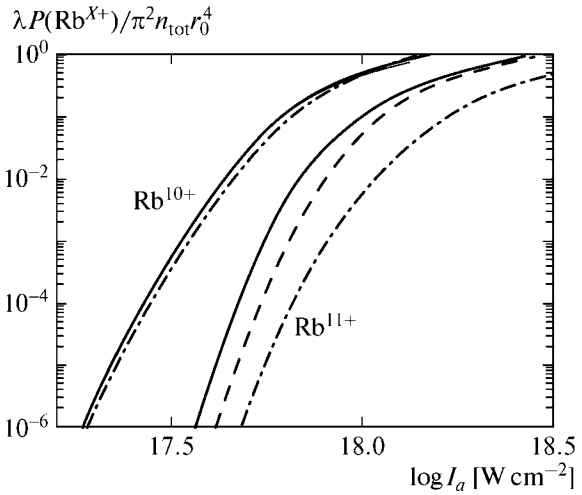

Fig. 6. Yield of Rb^{10+} and Rb^{11+} ions integrated over the focal volume. The notation is the same as that in Fig. 1.

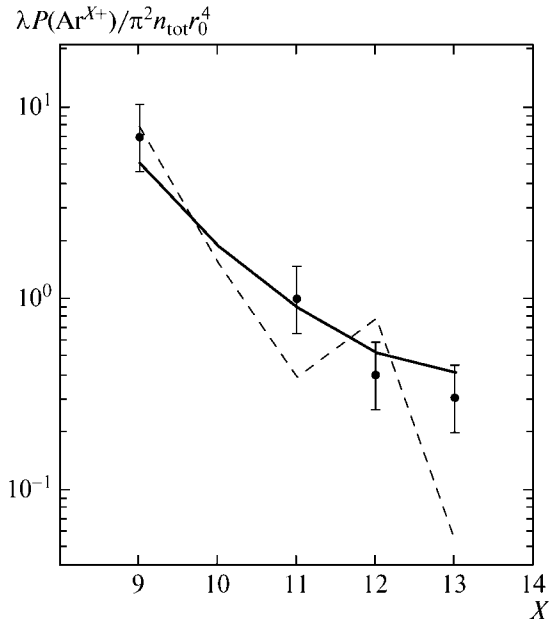

Fig. 7. Yield of Ar^{9+}... Ar^{13+} ions integrated over the focal volume versus ion charge. The absolute radiation intensity is 2.6×10^{19} W cm^{-2}. The experimental results (dots) were taken from [3]. In the experiment, the Ar^{11+} yield was taken as unity. The solid and dashed lines correspond to the single-electron inelastic tunneling and ADK models, respectively. The results of our calculations were reduced by a factor of 1.14.

the single-electron inelastic tunneling effect. The results are presented in Fig. 7.

As we see, the results of our calculations based on the many-body tunneling model agree well with the experimental data. The results obtained with the ADK model agree with the experiment much more poorly and depend on ion charge nonmonotonically.

Note the following fact: the authors of [3] had to reduce the intensity used in the ADK model by half to interpret the experimental results. When the inelastic tunneling model is used, no change in intensity is required, as in the case under consideration, or this change will be considerably smaller (no more than 5% in [19]).

The excess of the Ar^{12+} yield above the Ar^{11+} one when the ADK model is used is attributable to a two-fold difference between the maximum values of their populations at equal volumes occupied by these ions inside the focal region. The structure of the electronic spectra for these ions is responsible for such a nonuniform population of charge states in the ADK model. Figure 8 shows the difference between the first ionization potentials of neighboring unexcited ions (Ar^{X+} and $Ar^{(X-1)+}$). This difference increases monotonically with ion charge. Ar^{11+} constitutes an exception. At this ion charge, the dependence presented in Fig. 8 reaches a noticeable maximum due to a significant difference in the structure of the shells filled by more or less than half. As a result, the Coulomb pre-exponential factor in Eq. (1) for Ar^{10+} ions decreases by a factor of 1.5 compared to Ar^{11+}. Thus, the Ar^{11+} population found in the ADK model turns out to be poor. The physically not quite clear excess of the yield of higher-charge ions above that of lower-charge ones is a consequence of this fact. Such anomalies are presented, for example, in [3–5, 7]. Allowance for the inelastic channels removes such anomalies, because, as a result, the maximum populations become approximately equal and the MCI yield in a Gaussian beam begins to decrease monotonically with increasing ion charge.

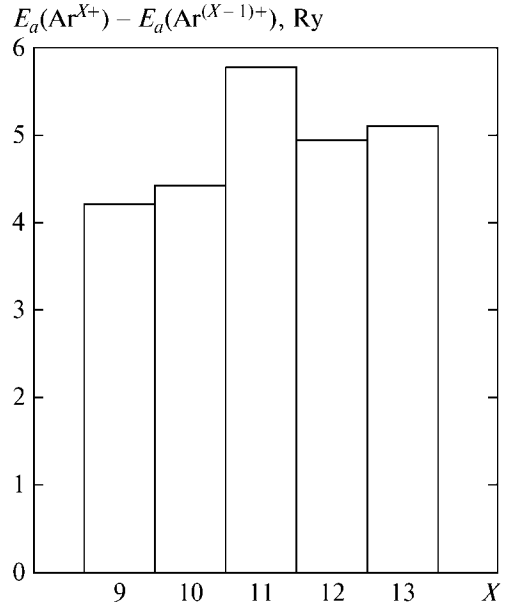

Fig. 8. Difference between the ionization potentials of neighboring Ar^{X+} ions ($X = 8, ..., 13$).

6. CONCLUSIONS

The results of our calculations presented here and in [18, 19] and confirmed by the experimental results [3, 23, 24] show that the main mechanism determining the difference between the many-body and single-body models for the formation of multiply charged ions in a laser field is the inelastic tunneling effect, which is significant for all the real laser intensities that lead to the formation of ions with a charge of 2 or higher. Ar^{9+}...Ar^{13+}, Kr^{19+}...Kr^{23+}, Rb^{10+}, and Rb^{11+} ions were used as an example to show that the collective two-electron tunneling effect, which changes the total Rb ion formation probability up to one order of magnitude and the yield of Ar and Kr ions by more than a factor of 2, becomes significant at a radiation intensity exceeding $10^{17.5}$ W cm^{-2}. For comparison, note that relativistic effects change the tunneling probability by an order of magnitude in hydrogen-like ions only at $Z \gtrsim 40$ [16]. We showed that the single-body and many-body models could lead to a qualitative difference between the results.

ACKNOWLEDGMENTS

This work was supported by the Russian Foundation for Basic Research (project no. 08-02-00337).

APPENDIX A

Ionic Wave Functions

While considering the interaction of outer d electrons of an ion with laser radiation, it is admissible to use the LS coupling approximation for ion charges $Z \lesssim 20$. The state of the l^k ($k \le 10$) shell is characterized by the set of quantum numbers ($aSLJM_J$). Here, J and M_J are, respectively, the total angular momentum of the shell and its projection (in our case, the quantization axis is chosen along the polarization vector of the laser radiation, $\mathbf{J} = \mathbf{L} + \mathbf{S}$, $\mathbf{L}$ and $\mathbf{S}$ are the total orbital momentum and spin, respectively), a are the additional quantum numbers for the classification of multielectron terms at $l \ge 2$. For the d shell, $a = v \le k$ is the so-called seniority number of the electronic configuration. It is the minimum number of electrons for which the state with given quantum numbers S and L appear for the first time. Since a free atom is spherically symmetric, the total energy of the shell does not depend on the magnetic quantum number M_J. Thus, the energy of any term of the l^k configuration is completely determined by the set of quantum numbers ($aSLJ$).

Let $\mathbf{r}_q$ be the radius vector of the qth electron, $\xi_q = (\mathbf{r}_q\sigma_q)$ is the set of its spatial and spin coordinates, $\xi^{(k)} = (\xi_1, ..., \xi_k)$ is the set of coordinates in the k-electron configuration. It is convenient to construct the wave function of the l^k shell in coordinate representation with certain values of the projection of the total spin M_S and total orbital angular momentum M_L:

$$\langle \xi^{(k)} | l^k(aSL) M_S M_L \rangle. \tag{A.1}$$

In the single-body approximation, the wave function (A.1) is expressed by a linear combination of function (A.1) of the l^{k-1} shell:

$$\begin{aligned}\langle \xi^{(k)} | l^k(aSL) M_S M_L \rangle &= R(r_k) Y_{lm_k}(\hat{\mathbf{r}}_k)_{\mu_k}(\sigma_k) \\ &\times \sum_{a', S', L'} C^{SM_S}_{S'M_S 1/2\mu_k} C^{LM_L}_{L'M_L lm_k} \\ &\times \langle l^{k-1}(a'S'L') l | l^k(aSL) \rangle \\ &\times \langle \xi^{(k-1)} | l^{k-1}(a'S'L') M_{S'} M_{L'} \rangle.\end{aligned} \tag{A.2}$$

Here, $R(r)$ is the radial wave function, $\chi(\sigma)$ is the spin function, $\langle l^{k-1}(a'S'L') l | l^k(aSL) \rangle$ is the fractional parentage coefficient. Their tables for $k = 3...5$ were first obtained in [37]. These coefficients provide antisymmetry of the wave function relative to the permutation of any pair (ξ_i, ξ_j). In the l^2 configuration, the fractional parentage coefficients become one and zero at even and odd $S + L$, respectively. If, alternatively, the l shell is filled with only one electron, then the sum in (A.2) become one. At a given k, the wave functions (A.1) are orthogonal and normalized to unity:

$$\begin{aligned}&\langle l^k(a'S'L') M_{S'} M_{L'} | l^k(aSL) M_S M_L \rangle \\ &\quad = \delta_{a'a} \delta_{S'S} \delta_{L'L} \delta_{M_{S'} M_S} \delta_{M_{L'} M_L}.\end{aligned} \tag{A.3}$$

Let us enumerate the permitted sets of (aSL) for various p^k and d^k configurations in spectroscopic notation (the seniority is indicated at the bottom left):

$$p^0: {}^1S;\ p^1: {}^2P;\ p^2: {}^3P, {}^1D, {}^1S;\ p^3: {}^4S, {}^2D, {}^2P;$$

$$d^0: {}^1S;\ d^1: {}^2D;\ d^2: {}_0{}^1S, {}^3P, {}^1D, {}^3F, {}^1G;\ d^3: {}^2P, {}^4P,$$

$${}_1{}^2D, {}^2D, {}^2F, {}^4F, {}^2G, {}^2H;$$

$$d^4: {}_0{}^1S, {}^1S, {}_2{}^3P, {}^3P, {}_2{}^1D, {}^1D, {}^3D, {}^5D, {}^1F, {}_2{}^3F, {}^3F,$$

$${}_2{}^1G, {}^1G, {}^3G, {}^3H, {}^1I;$$

$$d^5: {}^2S, {}^6S, {}_3{}^2P, {}_3{}^4P, {}_1{}^2D, {}_3{}^2D, {}^2D, {}^4D, {}_3{}^2F, {}^2F, {}_3{}^4F,$$

$${}_3{}^2G, {}^2G, {}^4G, {}_3{}^2H, {}^2I.$$

If the l^k shell is filled by more than half ($k = 2l + 2$, $2l + 3$, ..., $4l + 2$), then the same sets of (aSL) as those for the l^{4l+2-k} configuration are admissible for it. In this case, the fractional parentage coefficients are calculated from the recurrence formula [37]

$$\begin{aligned}\langle l^{k-1}(a'S'L') l | l^k(aSL) \rangle &= (-1)^{S+S'+L+L'-l+1/2} \\ &\times \left[\frac{4l+3-k}{k} \frac{2S'+1}{2S+1} \frac{2L'+1}{2L+1}\right]^{1/2} \\ &\times \langle l^{4l+2-k}(aSL) l | l^{4l+3-k}(a'S'L') \rangle.\end{aligned}$$

The states $|l^k(aSL)JM_J\rangle$ can be obtained from (A.1) in accordance with the rule for the vector addition of angular momenta:

$$|l^k(aSL)JM_J\rangle = \sum_{M_S, M_L} |l^k(aSL)M_SM_L\rangle C^{JM_J}_{LM_LSM_S}. \quad \text{(A.4)}$$

APPENDIX B

Overlap Integrals

The many-body structure of the ionic wave functions enters into the tunneling ionization probability via the square of the overlap integral Q. Calculating the overlap integral $\tilde{Q}$ for the tunneling N-electron transition from an initial state with k electrons

$$|l^k(a_kS_kL_k)M_{S_k}M_{L_k}\rangle$$

to a final state with $k-N$ electrons

$$|l^{k-N}(a_{k-N}S_{k-N}L_{k-N})M_{S_{k-N}}M_{L_{k-N}}\rangle$$

in representation (A.1) seems more convenient. We will neglect the change in the wave functions of the inner, completely closed electronic shells.[2]

For arbitrary k and N, Eq. (A.2) can be represented by a successive N-fold transformation as an expansion in terms of the basis of functions $\langle\xi^{(k-N)}|l^{k-N}(a_{k-N}S_{k-N}L_{k-N})M_{S_{k-N}}M_{L_{k-N}}\rangle$:

$$\langle\xi^{(k)}|l^k(a_kS_kL_k)M_{S_k}M_{L_k}\rangle = \sum_{[(aSL)M_SM_L]_{k-N}} \sum_{\text{all } m\mu} \tilde{Q}^{(m_{k-N+1}\mu_{k-N+1}, \ldots, m_k\mu_k)}_{\{lkN;\,[(aSL)M_SM_L]_{k-N},\,[(aSL)M_SM_L]_k\}}$$

$$\times \prod_{q=k-N+1}^{k} R(r_q)Y_{lm_q}(\hat{\mathbf{r}}_q)\chi_{\mu_q}(\sigma_q)\langle\xi^{(k-N)}|l^{k-N}(a_{k-N}S_{k-N}L_{k-N})M_{S_{k-N}}M_{L_{k-N}}\rangle.$$

Here, $(m_q\mu_q)$ is the set of orbital and spin angular momentum projections for the emitted electrons. We denote

$$[\alpha\beta\ldots]_i \equiv (\alpha_i, \beta_i, \ldots).$$

The expansion coefficients $\tilde{Q}$ will be the corresponding overlap integrals. They can be easily expressed using the recurrence relation

$$\tilde{Q}^{(m_{k-N+1}\mu_{k-N+1}, \ldots, m_k\mu_k)}_{\{lkN;\,[(aSL)M_SM_L]_{k-N},\,[(aSL)M_SM_L]_k\}} = \sum_{[aSL]_{k-N+1}} \langle l^{k-N}([aSL]_{k-N})l|l^{k-N+1}([aSL]_{k-N+1})\rangle$$

$$\times C^{L_{k-N+1}M_{L_{k-N+1}}}_{L_{k-N}M_{L_{k-N}}lm_{k-N+1}} C^{S_{k-N+1}M_{S_{k-N+1}}}_{S_{k-N}M_{S_{k-N}}1/2\mu_{k-N+1}} \tilde{Q}^{(m_{k-N+2}\mu_{k-N+2}, \ldots, m_k\mu_k)}_{\{lkN-1;\,[(aSL)M_SM_L]_{k-N+1},\,[(aSL)M_SM_L]_k\}}. \quad \text{(B.1)}$$

At $N=0$, we assume here that

$$\tilde{Q}_{\{lk0;\,[(aSL)M_SM_L]_k,\,[(aSL)M_SM_L]_k\}} = 1.$$

Quantities (B.1) have the following properties:

(1) In accordance with the Pauli exclusion principle, they change the sign after the permutation of any pair of indices $(m_q\mu_q)$ corresponding to the emitted electrons:

$$\tilde{Q}^{(\ldots, m_i\mu_i, \ldots, m_j\mu_j, \ldots)}_{\{\ldots\}} = -\tilde{Q}^{(\ldots, m_j\mu_j, \ldots, m_i\mu_i, \ldots)}_{\{\ldots\}}. \quad \text{(B.2)}$$

(2) The orthogonality relation (A.3) leads to the fulfillment of the following sum rule:

$$\sum_{[(aSL)M_SM_L]_{k-N}} \sum_{\text{all } m\mu} \left[\tilde{Q}^{(m_{k-N+1}\mu_{k-N+1}, \ldots, m_k\mu_k)}_{\{lkN;\,[(aSL)M_SM_L]_{k-N},\,[(aSL)M_SM_L]_k\}}\right]^2 = 1. \quad \text{(B.3)}$$

The set of quantities (B.1) can be tabulated using any computer algebra system. Relations (B.2) and (B.3) can be used to verify the results.

[2] Below, this approximation of "frozen" inner shells will be used everywhere.

The overlap integrals Q between the states $|l^k(aSL)JM_J\rangle$ can be obtained from $\tilde{Q}$ using Eq. (A.4). Using the orthogonality condition for the Clebsch–Gordan coefficients, we obtain

$$[Q^{(m_{k-N+1},\ldots,m_k)}_{\{lkN;\,[(aSL)M_LJ]_{k-N},\,[(aSL)M_LJ]_k\}}]^2 = \sum_{(M_SM_J)_{k-N}} \sum_{(M_SM_J)_k} \sum_{\text{all }\mu} \left[C^{J_kM_{J_k}}_{L_kM_{L_k}S_kM_{S_k}}\right]^2 \times \left[C^{J_{k-N}M_{J_{k-N}}}_{L_{k-N}M_{L_{k-N}}S_{k-N}M_{S_{k-N}}}\right]^2 [\tilde{Q}^{(m_{k-N+1}\mu_{k-N+1},\ldots,m_k\mu_k)}_{\{lkN;\,[(aSL)M_SM_L]_{k-N},\,[(aSL)M_SM_L]_k\}}]^2. \quad \text{(B.4)}$$

Since the tunneling ionization probability does not depend on the spin projection, the summation in Eq. (B.4) is performed over the corresponding quantum numbers.

Thus, to calculate the overlap integrals in the "frozen"-core approximation, it will suffice to use the main formalism of the theory of angular momentum. It is appropriate to take the fractional parentage coefficients from the original source [37], because they are given with errata in existing monographs (see, e.g., [38]).

REFERENCES

1. E. A. Chowdhury, C. P. J. Barty, and B. C. Walker, Phys. Rev. A: At., Mol., Opt. Phys. **63**, 042712 (2001).
2. M. Dammasch, M. Dörr, U. Eichmann, E. Lenz, and W. Sandner, Phys. Rev. A: At., Mol., Opt. Phys. **64**, 061402 (2001).
3. K. Yamakawa, Y. Akahane, Y. Fukuda, M. Aoyama, N. Inoue, and H. Ueda, Phys. Rev. A: At., Mol., Opt. Phys. **68**, 065 403 (2003).
4. K. Yamakawa, Y. Akahane, Y. Fukuda, M. Aoyama, N. Inoue, H. Ueda, and T. Utsumi, Phys. Rev. Lett. **92**, 123 001 (2004).
5. E. Gubbini, U. Eichmann, M. P. Kalashnikov, and W. Sandner, J. Phys. B: At., Mol. Opt. Phys. **38**, L87 (2005).
6. S. Palaniyappan, A. DiChiara, I. Ghebregziabher, E. L. Huskins, A. Falkowski, D. Pajerowski, and B. C. Walker, J. Phys. B: At., Mol. Opt. Phys. **39**, S357 (2006).
7. E. Gubbini, U. Eichmann, M. P. Kalashnikov, and W. Sandner, J. Phys. B: At., Mol. Opt. Phys. **39**, S381 (2006).
8. A. D. DiChiara, I. Ghebregziabher, R. Sauer, J. Waesche, S. Palaniyappan, B. L. Wen, and B. C. Walker, Phys. Rev. Lett. **101**, 173 002 (2008).
9. L. D. Landau and E. M. Lifshitz, *Course of Theoretical Physics*, Vol. 2: *The Classical Theory of Fields* (Fizmatlit, Moscow, 2000; Butterworth–Heinemann, Oxford, 2000).
10. M. Yu. Kuchiev, Pis'ma Zh. Eksp. Teor. Fiz. **45** (7), 319 (1987) [JETP Lett. **45** (7), 404 (1987)].
11. P. B. Corkum, Phys. Rev. Lett. **71**, 1994 (1993).
12. L. V. Keldysh, Zh. Eksp. Teor. Fiz. **47**, 1945 (1964) [Sov. Phys. JETP **20**, 1307 (1964)].
13. B. M. Smirnov and M. I. Chibisov, Zh. Eksp. Teor. Fiz. **49**, 841 (1965) [Sov. Phys. JETP **22**, 585 (1965)].
14. A. M. Perelomov, V. S. Popov, and M. V. Terent'ev, Zh. Eksp. Teor. Fiz. **50** (5), 1393 (1966) [Sov. Phys. JETP **23** (5), 924 (1966)].
15. M. V. Ammosov, N. B. Delone, and V. P. Krainov, Zh. Eksp. Teor. Fiz. **91** (6), 2008 (1986) [Sov. Phys. JETP **64** (6), 1191 (1986)].
16. N. Milosevic, V. P. Krainov, and T. Brabec, Phys. Rev. Lett. **89**, 193 001 (2002).
17. V. S. Popov, B. M. Karnakov, V. D. Mur, and S. G. Pozdnyakov, Zh. Eksp. Teor. Fiz. **129** (5), 871 (2006) [JETP **102** (5), 760 (2006)].
18. A. S. Kornev, E. B. Tulenko, and B. A. Zon, Phys. Rev. A: At., Mol., Opt. Phys. **68**, 043 414 (2003).
19. A. S. Kornev, E. B. Tulenko, and B. A. Zon, Phys. Rev. A: At., Mol., Opt. Phys. **69**, 065 401 (2004).
20. B. A. Zon, Zh. Eksp. Teor. Fiz. **118** (5), 1041 (2000) [JETP **91** (5), 899 (2000)].
21. B. A. Zon, Zh. Eksp. Teor. Fiz. **116** (2), 410 (1999) [JETP **89** (2), 219 (1999)].
22. U. Eichmann, M. Dörr, M. Maeda, W. Becker, and W. Sandner, Phys. Rev. Lett. **84**, 3550 (2000).
23. D. N. Fittinghoff, P. R. Bolton, B. Chang, and K. C. Kulander, Phys. Rev. A: At., Mol., Opt. Phys. **49**, 2174 (1994).
24. W. A. Bryan, S. L. Stebbings, J. McKenna, E. M. L. English, M. Suresh, J. Wood, B. Srigengan, I. C. E. Turcu, J. M. Smith, E. J. Divall, C. J. Hooker, A. J. Langley, J. L. Collier, I. D. Williams, and W. R. Newell, Nat. Phys. **2**, 379 (2006).
25. A. S. Kornev, E. B. Tulenko, and B. A. Zon, Phys. Rev. A: At., Mol., Opt. Phys. **79**, 063 405 (2009).
26. R. Taïeb, V. Véniard, and A. Maquet, Phys. Rev. Lett. **87**, 053002 (2001).
27. E. Gubbini, U. Eichmann, M. P. Kalashnikov, and W. Sandner, Phys. Rev. Lett. **94**, 053602 (2005).
28. Ch. Jungen, *Molecular Applications of Quantum Defect Theory* (Institute of Physics, Bristol, 1996).
29. V. E. Chernov, D. L. Dorofeev, I. Yu. Kretinin, and B. A. Zon, Phys. Rev. A: At., Mol., Opt. Phys. **71**, 022505 (2005).
30. T. A. Carlson, Phys. Rev. **156**, 147 (1967).
31. A. S. Kornev, I. Yu. Kretinin, and B. A. Zon, Laser Phys. **19**, 231 (2009).

32. Yu. Ralchenko, A. E. Kramida, J. Reader, and NIST ASD Team, *NIST Atomic Spectra Database (Version 3.1.5)* (National Institute of Standards and Technology, Gaithersburg, Maryland, United States, 2008); http://physics.nist.gov/asd3.
33. W. A. Bryan, S. L. Stebbings, E. M. L. English, T. R. J. Goodworth, W. R. Newell, J. McKenna, M. Suresh, B. Srigengan, I. D. Williams, I. C. E. Turcu, J. M. Smith, E. J. Divall, C. J. Hooker, and A. J. Langley, Phys. Rev. A: At., Mol., Opt. Phys. **73**, 013407 (2006).
34. M. A. Walker, P. Hansch, and L. D. Van Woerkum, Phys. Rev. A: At., Mol., Opt. Phys. **57**, R701 (1998).
35. A. l'Huillier, L. A. Lompre, G. Mainfray, and C. Manus, Phys. Rev. A: At., Mol., Opt. Phys. **27**, 2503 (1983).
36. A. A. Sorokin, S. V. Bobashev, T. Feigl, K. Tiedtke, H. Wabnitz, and M. Richter, Phys. Rev. Lett. **99**, 213002 (2007).
37. G. Racah, Phys. Rev. **63**, 367 (1943).
38. I. I. Sobel'man, *Introduction to the Theory of Atomic Spectra* (Fizmatlit, Moscow, 1963; Pergamon, New York, 1972).